

MCANet: A Multi-Scale Class-Specific Attention Network for Multi-Label Post-Hurricane Damage

Assessment using UAV Imagery

Zhangding Liu,¹ Neda Mohammadi,² and John E. Taylor^{3*}

¹Ph.D. Student, School of Computational Science and Engineering, Georgia Institute of Technology, 790 Atlantic

Dr NW, Atlanta, GA 30332, United States; e-mail: zliu952@gatech.edu

²Sydney Horizon Fellow, The University of Sydney, NSW 2006, Australia; e-mail:

neda.mohammadi@sydney.edu.au

²School of Civil and Environmental Engineering, Georgia Institute of Technology, 790 Atlantic Dr NW, Atlanta,

GA, 30332, United States; e-mail: nedam@gatech.edu

^{3*}Professor, School of Civil and Environmental Engineering, Georgia Institute of Technology, 790 Atlantic Dr

NW, Atlanta, GA, 30332, United States; e-mail: jet@gatech.edu (corresponding author)

ABSTRACT

Hurricanes are among the most destructive natural disasters, causing widespread infrastructure damage, displacing populations, and leading to significant economic losses. Timely and accurate assessment of post-hurricane damage is critical for effective disaster response and recovery. However, existing CNN-based methods are limited in capturing multi-scale spatial features and distinguishing between visually similar or co-occurring damage types. To address these limitations, we introduce MCANet, a multi-label classification framework that learns multi-scale representations while adaptively attending to spatially relevant regions for each damage category. The architecture integrates a Res2Net-based hierarchical backbone, which enriches spatial context across multiple spatial scales, with a multi-head class-specific residual attention module that enhances discrimination between damage types.

The multi-head design allows each attention branch to focus at different spatial granularities, improving the model's ability to balance local detail and global context. We evaluated MCANet on the RescueNet dataset, comprising 4,494 UAV images collected after Hurricane Michael. MCANet achieves a mean average precision (mAP) of 91.75%, outperforming baselines including ResNet, Res2Net, VGG, MobileNet, EfficientNet, and ViT. Notably, the multi-head attention strategy further boosts performance, reaching an mAP of 92.35% with eight heads, and improves average precision for challenging classes such as Road Blocked by over 6%. In addition, class activation mapping visualizations validate MCANet's ability to localize damage-relevant regions, demonstrating model interpretability. The outputs generated by MCANet can be applied to post-disaster risk mapping, emergency routing, and digital twin-based disaster response systems. Future research could integrate disaster-specific knowledge graphs and multimodal large language models to enhance MCANet's adaptability to unseen disaster types and enrich its semantic understanding in real-world decision-making systems.

Key words

Multi-label classification; Attention mechanism; Post-hurricane damage assessment; Deep learning; Disaster response

1. Introduction

Hurricanes are among the most destructive natural disasters, severely impacting communities across the United States by causing widespread infrastructure damage, service disruption, population displacement, and significant economic losses (Balaguru et al. 2023; Grinsted et al. 2019; Klotzbach et al. 2018; Young and Hsiang 2024). From 1900 to 2017, the United States was impacted by 197 hurricanes, resulting in 206 landfalls. When

adjusted to 2018 economic conditions, the total damage from these events amounts to nearly \$2 trillion, averaging close to \$17 billion in losses per year (Weinkle et al. 2018). Beyond economic losses, hurricanes also significantly disrupt human mobility, with studies showing short-distance trips increasing and long-distance travel sharply decreasing during disasters (Wang and Taylor 2014, 2016). As climate change progresses and coastal populations grow, hurricane-related losses are expected to continue to increase (Emanuel 2005; Jing et al. 2024). This underscores the need to develop tools that can automatically classify and assess post-disaster infrastructure damage to support emergency response and minimize losses.

Timely and accurate classification of post-hurricane damage is vital for coordinating emergency response efforts, prioritizing the allocation of resources, and facilitating rapid recovery (Al Shafian and Hu 2024; Kaur et al. 2021; Sun and Huang 2023). Quick identification of the most severely impacted areas can guide rescue operations, ensuring that aid reaches the most vulnerable populations first (Chou et al. 2017). Additionally, a detailed understanding of the extent and type of damage is essential for infrastructure repair and reconstruction planning, enabling communities to restore essential services and return to normalcy as quickly as possible (Liu et al. 2022).

Current post-disaster damage assessment methods face several limitations that hinder timely and accurate decision-making. Ground-based surveys are often slow, labor-intensive, and geographically constrained, and they expose rescue teams to potential hazards (Aela et al. 2024; Einizinab et al. 2023; Ejaz and Choudhury 2024; Spencer et al. 2019). Satellite imagery provides broad regional coverage and is frequently used for large-scale assessments (Al Shafian and Hu 2024), but it suffers from low spatial resolution, reliance on clear weather, and limited viewing angles. Social media has emerged as a supplementary data source offering near real-time observations, but it is highly user-dependent, often lacks geotagging accuracy, and varies greatly in content quality (Salley et al. 2024). In contrast, Unmanned Aerial Vehicles (UAVs) provide high-resolution, near real-time

imagery with the ability to capture building and road level damage at flexible altitudes and angles, making it a promising tool for rapid and reliable post-disaster damage assessment.

Once high-quality imagery is collected, the next challenge is to accurately classify the observed damage. Unlike conventional image classification datasets such as ImageNet (Deng et al. 2009), where each image typically contains a single, well-defined object, post-disaster aerial imagery is more complex. A single image may exhibit multiple, coexisting damage types—such as collapsed buildings, road blockages, and flooded areas—each occupying different spatial regions and varying greatly in scale and visibility. Large-scale destruction may span the entire image, while smaller features like debris are confined to localized areas and often obscured by clutter. Despite this complexity, many existing models adopt a single-label multi-class classification approach, assigning only one dominant damage category to an image or patch (Cao and Choe 2020; Cheng et al. 2021; McCarthy et al. 2020). This oversimplification mirrors earlier practices in remote sensing, where traditional scene classification methods relied on representing each image with the most prominent terrain feature (Qi et al. 2020). High-resolution UAV imagery often contain multiple semantically rich object types within the same scene, rendering single-label assumptions inadequate for disaster contexts (Tseng 2023). As a result, single-label models tend to oversimplify real-world disaster scenes (Shao et al. 2018), where overlapping or interdependent damage types are common, and reduce model effectiveness for response planning. Although object detection and semantic segmentation models can support multi-label outputs, they require dense, pixel-level annotations that are labor-intensive and time-consuming—up to one hour per image in the RescueNet dataset (Rahnemoonfar et al. 2023; Sirhan et al. 2024). This high annotation cost hinders scalability in time-critical disaster scenarios. In contrast, multi-label classification offers a more practical solution: it relies on coarse image-level labels while still enabling recognition of multiple damage types within the same image.

Recent research has shown that multi-label learning holds significant promise in remote sensing and disaster informatics (Pitakaso et al. 2024; Stoimchev et al. 2023; Sumbul et al. 2019; Tseng 2023), yet several technical challenges remain. First, standard CNN-based models often lack robust multi-scale representation, making it difficult to detect both localized and large-scale damage patterns within the same scene (Kopiika et al. 2025; Zhou et al. 2023). Second, many models fail to incorporate class-specific spatial attention, which is crucial for distinguishing visually similar damage types—such as minor versus major building damage—in cluttered environments (Liu et al. 2025a; Sumbul and Demir 2020).

To address these limitations, we introduce multi-scale class-specific attention network (MCANet), a deep learning framework designed for multi-label post-hurricane damage classification using aerial imagery. MCANet integrates a Res2Net-based backbone to enhance hierarchical multi-scale feature extraction and a class-specific residual attention (CSRA) module to improve inter-class feature discrimination. By jointly modeling spatial resolution and semantic specificity, MCANet effectively captures overlapping and spatially diverse damage patterns. We validate MCANet on the RescueNet dataset (Rahnemoonfar et al. 2023), which contains UAV imagery collected after Hurricane Michael. Experimental results show that MCANet outperforms conventional baseline models such as ResNet (He et al. 2016), Res2Net (Gao et al. 2021), VGG (Simonyan and Zisserman 2015), MobileNet (Howard et al. 2017), EfficientNet (Tan and Le 2020), and ViT (Dosovitskiy et al. 2021) in both accuracy and precision, demonstrating its effectiveness in complex multi-label disaster scenes and its potential to support more effective post-disaster damage assessment.

The remainder of this paper is structured as follows. Section 2 reviews existing deep learning approaches for damage classification and outlines challenges in multi-label modeling for disaster imagery. Section 3 presents the proposed MCANet architecture in detail. Section 4 describes the experimental setup and analyzes the results. Section 5 discusses the contribution, limitations, and future work of this study. Section 6 concludes the paper.

2. Literature Review

2. 1. Deep Learning Approaches for Post-Hurricane Damage Classification

Recent advancements in deep learning have significantly enhanced automated damage classification of civil infrastructure (Tong et al. 2025). Early studies primarily focused on binary classification, typically distinguishing between "damaged" and "undamaged" structures. McCarthy et al. (2020) used multispectral satellite imagery to classify healthy versus degraded vegetation after Hurricane Irma. Similarly, Cao and Choe (2020) employed a convolutional neural network to distinguish flooded or damaged buildings from undamaged ones following Hurricane Harvey, achieving 97.08% accuracy. While effective, their study also noted key limitations of satellite imagery, including low spatial resolution and inconsistent label quality.

To support more detailed damage interpretation, researchers have advanced from binary to multi-class classification frameworks. Li et al. (2018) developed a semi-supervised approach combining Simple Linear Iterative Clustering segmentation, convolutional autoencoders, and a fine-tuned CNN to classify aerial image patches into five damage levels. Tested on post-Hurricane Sandy imagery, their method achieved an accuracy of 88.3%, demonstrating robustness with limited labeled data. Cheng et al. (2021) proposed a two-stage stacked preliminary damage assessment architecture using UAV footage from Hurricane Dorian. Their model classified building damage into six ordered levels (Level 0: no damage to Level 5: destroyed or under construction), reaching 61% accuracy and 90% within ± 1 level on seen data. Berezina and Liu (2022) implemented a coupled CNN with U-Net-based segmentation and ResNet classification on the xBD satellite dataset (Hurricane Michael), targeting four damage categories: undamaged, minor, major, and destroyed. Their model addressed class imbalance with focal loss and achieved 86.3% overall accuracy, outperforming traditional baselines while highlighting the difficulty of distinguishing visually similar classes.

Beyond classification, Pi et al. (2021) applied semantic segmentation and object detection to the Volan2019 UAV dataset, which includes pixel-level labels for nine disaster-related categories. Using Mask-RCNN and PSPNet, they achieved a mAP of 51.54% and a mean IoU of 32.17%. While their approach enables spatially detailed assessment, it highlights the high annotation cost and computational demands of segmentation-based methods. In this context, multi-label classification provides a practical alternative, requiring only image-level labels while still capturing multiple coexisting damage types within a scene.

2. 2. Multi-Label Classification in Disaster Damage Assessment

Multi-label classification has emerged as a powerful paradigm for analyzing complex visual scenes, particularly in remote sensing and disaster response contexts. Unlike single-label models, multi-label approaches can capture the co-occurrence of diverse categories within a single image, making them well-suited for tasks involving aerial or satellite imagery. This approach has demonstrated superior descriptive capabilities (Stoimchev et al. 2023; Tseng 2023) and has been widely adopted in applications such as land cover mapping (Sumbul and Demir 2020; You et al. 2023), image retrieval (Shao et al. 2020), and post-disaster data curation (Ho Ro et al. 2024; Pitakaso et al. 2024). The BigEarthNet benchmark (Sumbul et al. 2019) highlights the need for multi-label learning in remote sensing due to the heterogeneous nature of overhead images. In disaster informatics, Park et al. (2022) demonstrated the advantages of a multi-output CNN for post-earthquake image tagging, showing that unified multi-label models can improve classification efficiency and scalability in large reconnaissance datasets.

Post-disaster aerial imagery presents unique challenges due to the presence of multiple overlapping damage types—such as road blockages, building collapses, and debris—that vary in spatial scale, visibility, and location. These complex scenes often exhibit strong intra-class variation and inter-class similarity, which complicates the task of assigning accurate labels (Ro and Gong 2024). Moreover, damage indicators may appear

at different resolutions, ranging from regional flooding to fine-grained structural cracks, necessitating models that can reason across scales. Traditional CNN-based models often fall short in this regard, as they are typically limited by fixed receptive fields and lack mechanisms to effectively aggregate multi-scale context (Kopiika et al. 2025; Liu et al. 2025b). Two key limitations of conventional CNNs have been identified in this setting. First, poor multi-scale feature representation limits the ability to capture both local details and global patterns in disaster scenes. Second, weak feature discrimination—especially in cluttered or visually ambiguous regions—leads to confusion among overlapping damage types. Liu et al. (2025a) noted that standard CNNs struggle to differentiate visually similar classes without architectural enhancements, often misclassifying important disaster-related features. These shortcomings highlight the need for more adaptive models that can attend to class-specific information and extract features at multiple levels of granularity.

Recent research has attempted to address these limitations through attention mechanisms and multi-scale feature fusion. For example, You et al. (2023) introduced an attention-enhanced DenseNet using spatial and channel attention to better highlight relevant features. Similarly, Kaur et al. (2023) proposed a hierarchical transformer for building damage classification, fusing features across multiple resolutions and achieving strong results on the xBD benchmark. These studies highlight the promise of attention-aware, multi-scale models for improving robustness in disaster damage assessment. However, most existing models treat multi-scale representation and class-specific attention as isolated components, and few are designed to jointly address the spatial and semantic complexity of post-hurricane aerial imagery. These insights collectively motivate the need for unified, attention-aware architectures capable of learning multi-label representations that are both spatially precise and semantically expressive—requirements we address with our proposed MCANet framework.

3. Methods

This section introduces the MCANet for multi-label post-hurricane damage classification. Section 3.1 outlines the flowchart of the proposed framework. Section 3.2 describes the multi-scale feature extraction module, and then the class-specific residual attention module is detailed in Section 3.3. Finally, Section 3.4 describes the loss function in MCANet.

3. 1. Flowchart of the Proposed Approach

The proposed MCANet framework for multi-label post-hurricane damage classification integrates two key components, including a multi-scale feature extractor and a multi-head CSRA module. An overview of the MCANet architecture is presented in **Error! Reference source not found.**. Given a UAV image as input, the mutli-scale feature extractor Res2Net generates a feature tensor, denoted as $\mathbf{x} \in \mathbb{R}^{d \times h \times w}$, where d , h , and w correspond to the dimensionality, height, and width of the feature map, respectively. This tensor serves as the base representation of the input image, capturing rich multi-scale features. Next, the feature tensor \mathbf{x} is processed through C independent 1×1 convolutional layers, where C is the number of classes. Each 1×1 convolutional layer generates a class-specific score map of size $h \times w$, which represents the spatial distribution of scores for a specific class. These score maps are then stacked together to form a class-specific score tensor $\mathbf{R}_C \in \mathbb{R}^{C \times h \times w}$, with each channel corresponding to one class.

The residual attention mechanism is applied to refine each class-specific score tensor by calculating and applying attention weights for each class across spatial locations. This mechanism incorporates a temperature parameter T , which controls the sharpness of the attention scores. Following the application of residual attention, logits \hat{P}_{T_i} are generated for each attention head (i.e., class-specific branch), where $i \in \{1, 2, \dots, H\}$, and H represents the total number of heads. Each head is associated with a specific temperature T_i , enabling the network

to learn diverse attention behaviors across heads. This multi-head configuration ensures that features from different spatial and semantic perspectives are captured effectively, enhancing the model's capacity for multi-label classification.

The final logits \hat{P}_O are obtained by fusing the outputs from all attention heads. Specifically, the logits $\hat{P}_{T_1}, \hat{P}_{T_2}, \dots, \hat{P}_{T_H}$ are summed, with a shared weighting parameter λ used to balance the contributions from each head. This fusion process combines information from diverse attention heads, resulting in robust and comprehensive predictions.

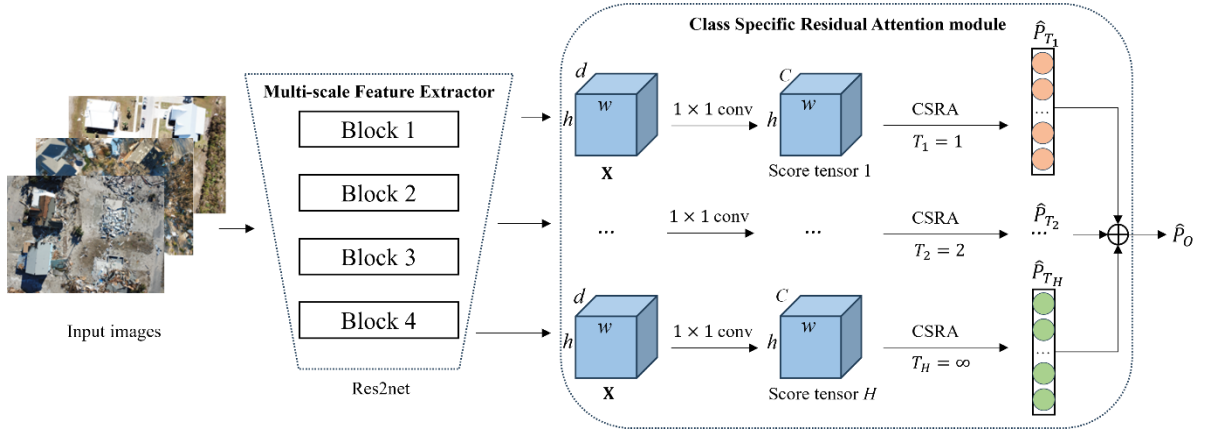


Fig. 1. Overview of the proposed MCANet for multi-label post-hurricane damage classification, integrating multi-scale feature extraction and a multi-head class-specific residual attention module.

3. 2. Multi-Scale Feature Extraction Module

This study employs the Res2Net architecture (Gao et al. 2021) as the feature extractor in MCANet, a variant network based on ResNet framework (He et al. 2016). ResNet and Res2Net share a similar overall architecture, but they differ in residual block design. As shown in Fig. 2, while ResNet uses residual connections to enable deep hierarchical learning, its standard residual blocks apply convolution operations with a fixed

receptive field, which limits its ability to model objects of varying sizes. In contrast, Res2Net enhances each residual block with a split-transform-merge strategy to capture information at multiple spatial scales.

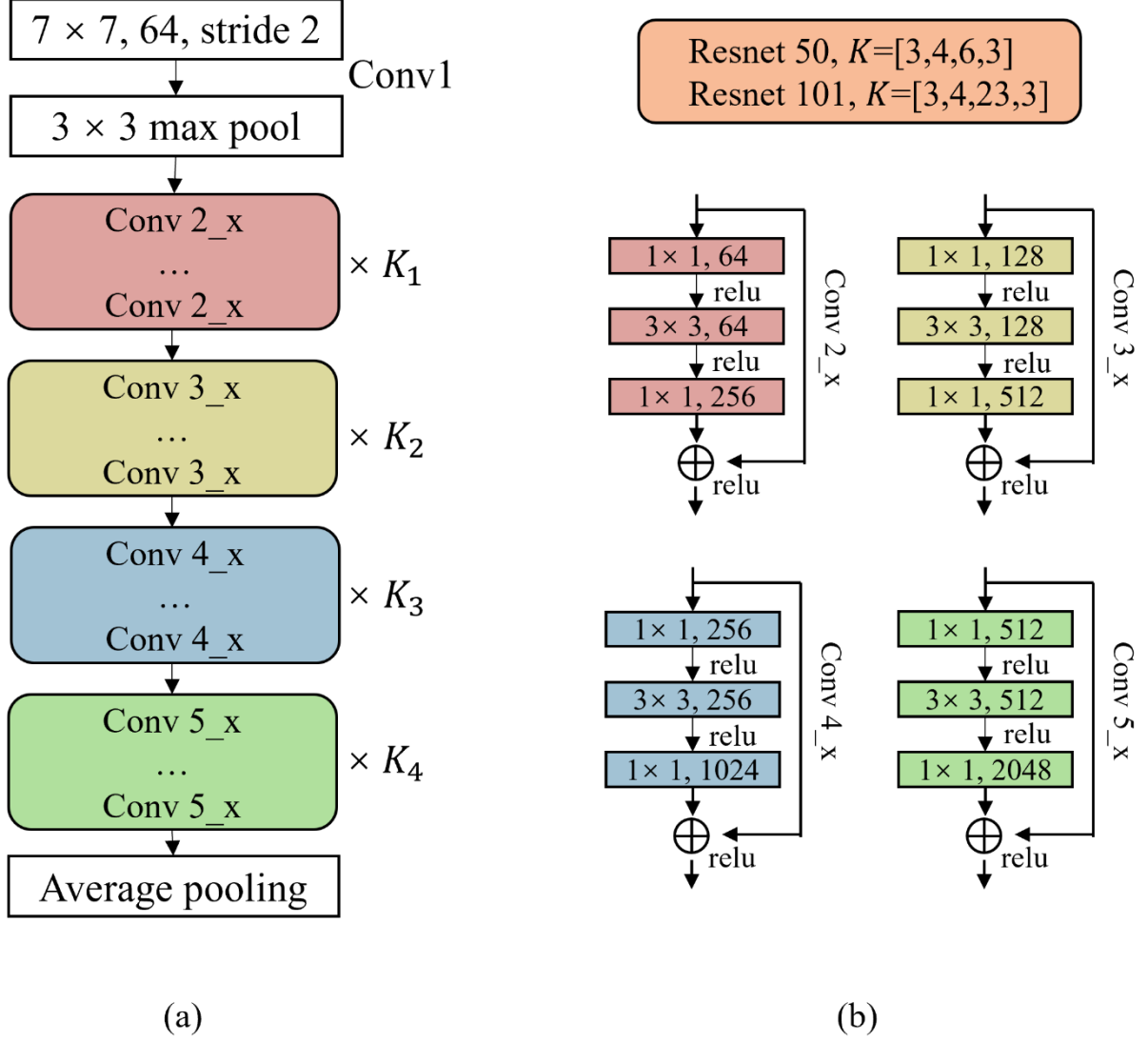


Fig. 2. (a) Overall architecture of both ResNet and Res2Net, both comprising four convolutional stages; ResNet 50 uses $K=[3,4,6,3]$ bottleneck blocks per stage, while ResNet 101 uses $K=[3,4,23,3]$. Both start with a 7×7 convolution and max pooling. (b) Residual block design of ResNet, where each block consists of a sequence of 1×1 , 3×3 , and 1×1 convolutions with relu and skip connections.

As illustrated in Fig. 3, the Res2Net block first applies a 1×1 convolution to the input feature map, then splits it into multiple subsets, each processed by an independent 3×3 convolution with its own receptive field. These outputs are sequentially aggregated via additional 1×1 convolutions, with a scale parameter controlling the number

of subsets (e.g., scale = 4 produces four groups, each capturing a different level of detail). This design allows a single block to model fine-to-coarse features and capture hierarchical spatial information more effectively. Such multi-scale representation learning is particularly beneficial for post-hurricane UAV imagery, where damaged buildings, blocked roads, and flooded areas vary greatly in size, often overlap, and require different contextual cues for accurate identification. By embedding multi-scale modeling into each residual block, Res2Net provides a strong foundation for robust and accurate multi-label classification in complex disaster environments.

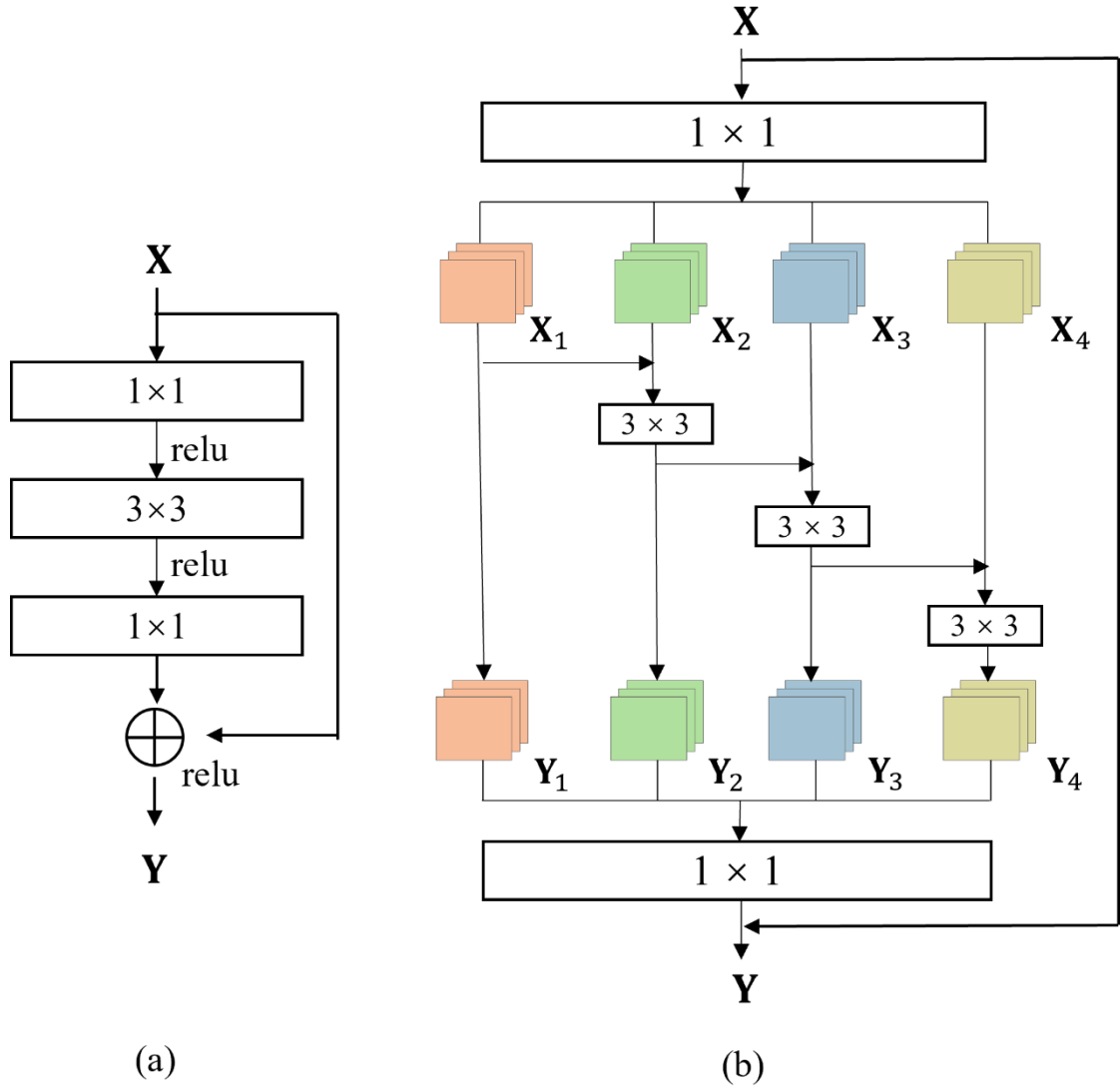


Fig. 3. Comparison between (a) ResNet residual block with a single-scale receptive field and (b) Res2Net residual block with intra-block multi-scale feature extraction.

3. 3. Class Specific Residual Attention Module

Some researchers have applied attention mechanisms to improve aerial image classification performance (Hua et al. 2020; Wang et al. 2021). However, few studies have explored the use of attention mechanisms in multi-label post disaster classification scenarios. To capture various regions that are occupied by objects belonging to different damage categories more efficiently, we utilize a CSRA module to integrate spatial attention. CSRA creates category-aware features for each class by introducing a spatial attention score, which is then merged with the class-agnostic average pooling feature (Zhu and Wu 2021).

Fig. 4 illustrates the class specific residual attention module. The process begins with extracting the input feature tensor \mathbf{x} from the feature extraction module mentioned in last section. Assuming an input image resolution of 448×448 , the convolutional layers in the feature extraction module downsample the spatial dimensions through a series of pooling and convolution operations. As a result, the feature tensor \mathbf{x} has a shape of $2048 \times 14 \times 14$, where 2048 corresponds to the number of feature channels, and 14×14 represents the spatial dimensions. This tensor can be flattened into 196 spatial regions, denoted as X_1, X_2, \dots, X_{196} , where $X_k \in \mathbb{R}^{2048}$ corresponds to the feature vector at the k -th spatial location.

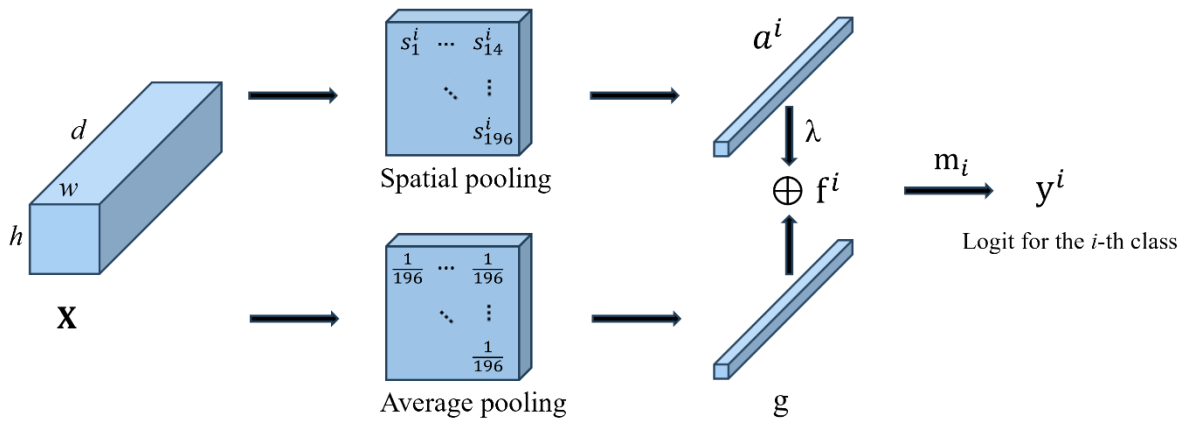


Fig. 4. Class specific residual attention module.

To capture class-specific spatial relevance, attention scores (Zhu and Wu 2021) for the i -th class and j -th location are computed using the following equation:

$$s_j^i = \frac{\exp(T \cdot X_j^T m_i)}{\sum_{k=1}^{h \times w} \exp(T \cdot X_k^T m_i)}, \quad (1)$$

where $\sum_{j=1}^{h \times w} s_j^i = 1$ ensures that the attention scores are normalized across all spatial locations, and $T > 0$ is a temperature parameter controlling the sharpness of the scoring. Here, the vector $m_i \in \mathbb{R}^{2048}$ represents the classifier weights for the i -th class. $X_j^T m_i$ represents the dot product between the feature vector at spatial location X_j (transposed for proper dimensionality) and the classifier weights m_i , reflecting how strongly the location is associated with the target class. The temperature parameter T adjusts the focus of attention: larger values of T result in sharper distributions, emphasizing a few key spatial locations, while smaller values produce smoother distributions, spreading the focus across a broader region. Assigning different T values to different attention heads allows the model to capture spatial dependencies at multiple levels of granularity.

The computed attention scores s_k^i are then used as weights to aggregate spatial features into a class-specific feature vector for the i -th class, as follows:

$$a^i = \sum_{k=1}^{h \times w} s_k^i X_k. \quad (2)$$

This weighted sum aggregates the spatial features across the image based on their relevance to the i -th class, effectively focusing on localized regions of importance for that class. Additionally, a global class-agnostic feature vector g is computed by averaging the feature tensor over all spatial locations:

$$g = \frac{1}{h \times w} \sum_{k=1}^{h \times w} X_k. \quad (3)$$

The global feature vector g provides a comprehensive representation of the entire image, capturing context without focusing on specific regions or classes. Finally, as shown in Fig. 4, the global feature vector g and the class-specific feature vector a^i are combined to produce the final class-specific feature vector for the i -th class:

$$f^i = g + \lambda a^i. \quad (4)$$

where λ is a hyperparameter that balances the contribution of global contextual features g and class-specific localized features a^i . This combination ensures that the model leverages both holistic and localized information to enhance classification performance, effectively addressing the challenges of multi-label image recognition.

To finalize the classification process, a fully connected layer serves as the classifier, with $m_i \in \mathbb{R}^d$ representing the weight vector corresponding to the i -th class. These weight vectors are utilized in conjunction with the class-specific feature vectors f^i to compute the logits for all classes. The logit for the i -th class is calculated as:

$$y^i = m_i^T f^i, \quad (5)$$

For the multi-label classification task, the logits are transformed using a sigmoid activation function. The sigmoid function is chosen over softmax function because it enables independent modeling of each class, a necessity in multi-label classification scenarios where multiple labels can simultaneously apply to a single instance. The sigmoid function transforms the network's output into values between 0 and 1, representing the predicted probability for each class. To obtain the final binary predictions, a threshold of 0.5 is applied to the sigmoid outputs. Output values greater than or equal to 0.5 are classified as 1, indicating the presence of the corresponding class in the image, while values below 0.5 are classified as 0, indicating its absence. This thresholding operation results in a binary vector like $[1, 0, 1, \dots, 0]$, where each 1 signifies the presence of the corresponding label in the image and each 0 indicates its absence.

3. 4. Loss Function

We employ the binary cross-entropy loss function, as defined in equation (6), to calculate the loss between the predicted output \hat{y}_i and the actual binary labels y_i associated with each class. In this work, we adopt an independent-label multi-label setting, where multiple classes can be present in the same image. Accordingly, the binary cross-entropy loss is computed separately for each class and summed across all classes to obtain the loss for a single instance, which is then averaged over the batch to provide a stable optimization signal during training. The binary cross-entropy loss for a single instance is defined as

$$Loss(y, \hat{y}) = - \sum_{i=1}^N y_i \log \hat{y}_i + (1 - y_i) \log(1 - \hat{y}_i), \quad (6)$$

where N is the total number of classes. The loss is minimized using stochastic gradient descent with momentum.

4. Experiments and Results

4. 1. Data

Hurricane Michael, a category 5 storm that made landfall near Mexico Beach, Florida, on October 10, 2018, was one of the most intense hurricanes to strike the U.S. mainland, causing over \$25 billion in damages and resulting in 16 fatalities (Kennedy et al. 2020). The RescueNet dataset was collected with a small UAS platform after Hurricane Michael, including 4,494 RGB images with multi-label annotations across object types and damages (Rahnemoonfar et al. 2023). As described in **Error! Reference source not found.**, the dataset has six primary instance types including road, tree, building, water, vehicle, and pools. The road and building instance types include sub-classifications based on damage severity. The building damage was divided into four classifications: Building No Damage, Building MinorDamage, Building Major Damage, and Building Total Destruction. Road damage was divided into two classifications: Road Clear and Road Blocked. **Table 1** shows the total number of labels for each building damage level. Several representative UAV images and their corresponding multi-label annotations from the RescueNet dataset are presented in **Error! Reference source not found.**

Table 1. Damage classification in RescueNet.

Instance Type	Class name	Definition
Road	Road Clear	Roads that are undamaged, clear of water or debris
	Road Blocked	Roads that are flooded or blocked by debris
Tree	Tree	Individual trees or groups of trees
Building	Building No Damage	Buildings with roof damage that are either completely absent or very hardly observable.
	Building Minor Damage	Buildings with partially damaged roofs that permit the use of tarps as protection,

	Building Major Damage	Buildings with severely damaged roofs, either entirely or significantly.
	Building Total Destruction	Fully destroyed buildings with only the base remaining visible
Water	Water	Natural water reservoirs or caused by floods.
Vehicle	Vehicle	Trucks and cars.
Pool	Pool	Pools situated next to a building.

Table 1. Number of labels by building damage level.

Damage Level	Description	Number
L0	Building No Damage	4011
L1	Building Minor Damage	3119
L2	Building Major Damage	1693
L3	Building Total Destruction	2080



Building Total Destruction, water
Road-Blocked.



Building Minor Damage, Road-Clear.



Building No Damage, Vehicle,
Road-Clear, Tree.

Fig. 5. Example images and multi labels of RescueNet dataset.

4. 2. Implementation Details

To validate the performance of the proposed MCANet, we conducted a series of comparative experiments against several widely used backbone architectures. Specifically, we evaluated the model's effectiveness in multi-label hurricane damage classification by benchmarking it against ResNet (He et al. 2016), Res2Net (Gao et al. 2021), VGG (Simonyan and Zisserman 2015), MobileNet (Howard et al. 2017), EfficientNet (Tan and Le 2020), and Vision Transformer (ViT) (Dosovitskiy et al. 2021).

In each of our experiments, the RescueNet dataset was divided into two subsets with a ratio of 80% for training and 20% for testing. To augment the data, we apply random horizontal flip and random scaled cropping. We base our training parameter settings on established approaches in deep learning (Dosovitskiy et al. 2021; He et al. 2016; Zhu and Wu 2021). For the CSRA module and classifiers, a learning rate of 0.1 is selected, while a lower rate of 0.01 is set for the feature extraction module. To enhance training, a warmup scheduler is applied to both the baseline and CSRA models. The feature extraction module is initialized with ImageNet pretrained weights and trained for 30 epochs on RescueNet datasets. Consistent with prior work, the system employs a momentum of 0.9 coupled with a weight decay factor set at 0.0001. During training, all input images are resized into a fixed size 448×448.

4. 3. Evaluation Metrics

The primary approach of assessing classification performance of our model is to compare predicted labels to true labels, which can be quantified by four basic metrics, namely mean average precision (mAP), overall precision (OP), overall recall (OR), and overall F1-measure (OF1), following previous multi-label image classification studies (Wang et al. 2016; Chen et al. 2019; Gao and Zhou 2021).

For each category i , Average Precision (AP_i) measures the match between the predicted labels by the model and the actual labels, the calculation of AP is an approximation of the area under the precision-recall curve. The mAP measure is the average of AP across all categories, which is widely used to measure the overall performance of a model across all classes. OP represents the ratio of correct predictions to the total number of labels predicted by the model, while OR measures the proportion of correctly predicted labels out of all the actual ground truth labels. OF1 is the harmonic mean of precision and recall, which balances the relationship between

these two metrics. Among all these metrics, mAP and OF1 are the key metrics for evaluation. The formulas of these metrics are defined from equation (7) to (11) as below.

$$AP_i = \int_0^1 P_i(R) dR \quad (7)$$

$$mAP = \frac{1}{N} \sum_{i=1}^N AP_i \quad (8)$$

$$OP = \frac{\sum_i N_i^c}{\sum_i N_i^p} \quad (9)$$

$$OR = \frac{\sum_i N_i^c}{\sum_i N_i^g} \quad (10)$$

$$OF1 = \frac{2 \times OP \times OR}{OP + OR} \quad (11)$$

where $P_i(R)$ is the precision as a function of recall R , N is the total number of classes, AP_i represents the average precision for the i -th class. N_i^c is the number of images correctly predicted for the i -th class, N_i^p is the number of images predicted as positive for the i -th class, N_i^g is the number of ground truth images for the i -th class. For each image, a label is predicted as positive if its estimated probability exceeds the threshold of 0.5.

4. 4. Results and Analysis

Table 3 summarizes the quantitative comparison of MCANet with baseline models for multi-label post-hurricane damage classification. MCANet outperforms all competing methods across four key metrics, achieving a mAP of 91.75%, OP of 87.57%, OR of 86.31%, and OF1 of 86.93%. These results reflect the effectiveness of MCANet’s architecture in capturing complex, multi-scale, and co-occurring damage types. Among the baseline models, ViT performs notably well with a mAP of 90.76%, outperforming all convolutional baselines. Its self-attention-based mechanism allows it to model long-range dependencies more effectively than traditional CNNs.

However, MCANet still outperforms ViT in all four metrics, indicating the added benefit of incorporating multi-scale feature aggregation and class-specific attention mechanisms on top of a strong backbone. Within the convolutional models, Res2Net101 achieves the highest performance (mAP = 88.68%) likely due to its multi-scale feature extraction strategy, outperforming standard CNN backbones such as ResNet50 (mAP = 86.55%) and VGG19 (mAP = 85.08%).

The observed performance gaps underscore the limitations of conventional CNNs in capturing fine-grained semantic variations and modeling hierarchical spatial dependencies—critical requirements for reliable multi-label classification in disaster scenarios. In contrast, MCANet integrates a Res2Net-based hierarchical backbone with a CSRA mechanism, enabling the model to dynamically focus on salient features across different spatial scales and damage types.

Table 3. Performance comparison of different models in multi-label hurricane damage classification. The best performance in each column is indicated by the bold font.

Method	mAP	OP	OR	OF1
Resnet50	86.55	85.72	78.68	82.05
Resnet101	87.24	84.87	81.55	83.18
Res2net101	88.68	85.15	80.77	82.90
VGG19	85.08	81.92	79.14	80.50
MobileNet	87.33	84.08	79.53	81.74
EfficientNet	86.97	83.21	80.12	81.63
ViT	90.76	86.68	84.81	85.73
MCANet	91.75	87.57	86.31	86.93

Fig. 6 presents a heatmap summarizing the per-class performance metrics of MCANet for post-hurricane damage classification. The model exhibits strong performance across most damage categories. Notably, Tree, Road Clear, and Pool achieve the highest AP scores, reflecting their distinct and stable visual patterns in UAV

imagery, which make them easier to distinguish from other categories. Within the building-related classes, Building No Damage outperforms Building Minor Damage and Building Major Damage, likely due to a combination of class imbalance in the training data and the difficulty in distinguishing between adjacent damage levels that differ only subtly in visual appearance. Similarly, the Road Blocked category shows the weakest performance, with an AP of 71.56%, attributable to both its relatively low frequency in the dataset and the inherent visual complexity of blocked roads—often characterized by occlusions, scattered debris, and variable road conditions.

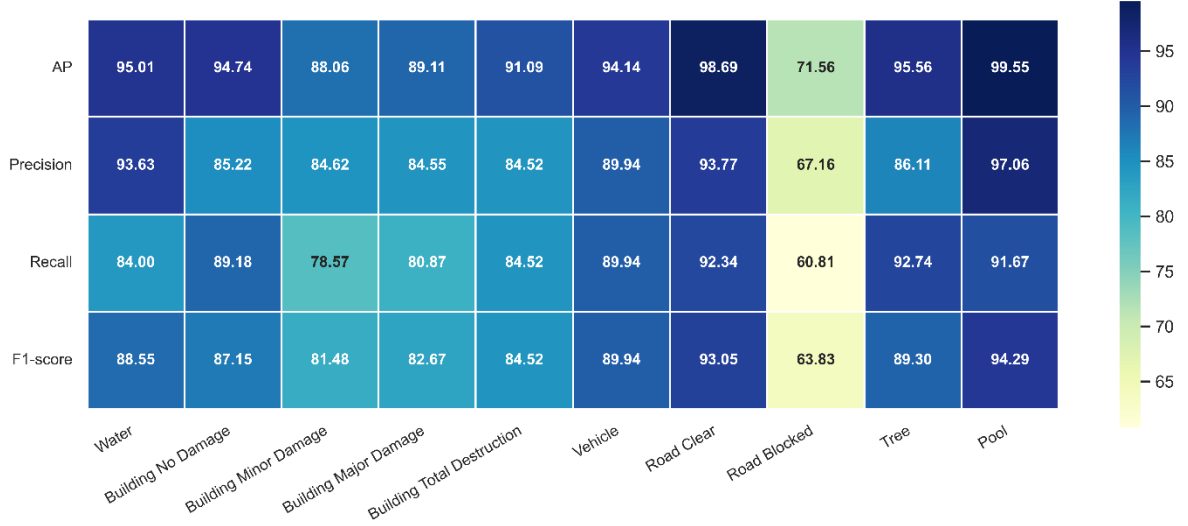


Fig. 6. Heatmap of per-class performance of MCANet on the RescueNet dataset, displaying precision, recall, F1-score, and AP for each damage category.

4. 4. 1. Multi-Head Attention

Our previous analysis demonstrated the effectiveness of MCANet in improving performance when configured with a single attention head in CSRA module. The attention mechanism is controlled by a single temperature parameter T , which modulates the sharpness of the softmax distribution across spatial locations. However, this fixed-temperature design imposes a trade-off: high T values encourage spatial selectivity but risk

ignoring contextual cues, while low T values promote global smoothing but may dilute class-specific saliency. Importantly, different damage categories often require different spatial focus patterns. For instance, Pool may benefit from sharp localization, whereas Blocked Roads may require broader contextual awareness. To address this, we incorporate a multi-head extension to CSRA, in which multiple attention heads operate in parallel, each with a distinct temperature setting (shown in Fig. 1). The temperature configuration for H heads is defined as:

$$T = \{1, 2, \dots, H - 1, 99\} \quad (12)$$

where the final head ($T = 99$) approximates uniform attention. This ensemble of heterogeneous attention distributions allows the model to capture a richer variety of spatial dependencies, from localized object boundaries to diffuse contextual patterns. The final classification logits are obtained by summing the outputs across all heads. Table 4 summarizes the performance of MCANet under different head configurations on the RescueNet dataset. As the number of attention heads increases, the model's mAP improves consistently, with the best result achieved at eight heads (mAP = 92.35%). This trend suggests that multi-head attention enables the model to better adapt to the diverse spatial characteristics inherent in post-hurricane aerial imagery.

Table 4. Impact of the number of attention heads in CSRA on mAP performance. The best result is indicated by the bold font.

Head number	1	2	4	8
mAP	91.75	91.77	91.86	92.35

To further understand the benefits of multi-head attention, we analyze per class performance improvements, focusing on the most challenging category Road Blocked. Table 5 shows that as the number of

attention heads increases, all performance metrics (AP, precision, recall, and F1-score) for the Road Blocked class consistently improve. Specifically, the AP improves from 71.56% at one head to 78.13% at eight heads, while the F1-score increases by more than 5 points. These gains suggest that the model’s ability to integrate both local and contextual cues via diverse attention heads is particularly beneficial for visually ambiguous and underrepresented categories.

Table 5. Performance of the “Road Blocked” class under different CSRA head configurations. The best result is indicated by the bold font.

Head number	AP	Precision	Recall	F1-score
1	71.56	67.16	60.81	63.83
2	73.23	64.47	66.22	65.33
4	75.03	67.95	71.62	69.74
8	78.13	68.92	68.92	68.92

4. 4. 2. Ablation Study

To evaluate the individual and combined contributions of the Res2Net101 backbone and the CSRA module, we conducted an ablation study using ResNet101 as the baseline. As summarized in Table 6, substituting ResNet101 with Res2Net101 alone yields a 1.44% increase in mAP, demonstrating the advantage of multi-scale feature extraction. However, this backbone modification results in a slight decline in recall (−0.78%) and F1 score (−0.28%), indicating that while Res2Net enhances spatial detail capture, it may fall short in maintaining global contextual sensitivity.

By integrating the CSRA module with Res2Net101 (i.e., forming MCANet), the model achieves the best overall performance, with mAP increasing by 5.11% relative to the baseline. Gains are also observed in overall precision ($\Delta\text{OP} = +1.53\%$), recall ($\Delta\text{OR} = +6.65\%$), and F1 score ($\Delta\text{OF1} = +4.11\%$). These results confirm that

the class-specific residual attention mechanism complements the multi-scale backbone by enabling adaptive focus on critical damage regions. Together, the two components form a robust architecture that enhances the accuracy of post-disaster multi-label damage classification.

Table 6. Ablation Study of Res2Net101 Backbone and CSRA Module on Model Performance. Δ mAP, Δ OP, Δ OR, Δ OF1 are computed relative to ResNet101 baseline. The bolded values indicate the best performance for each metric.

Method	mAP	Δ mAP	OP	Δ OP	OR	Δ OR	OF1	Δ OF1
Resnet101	87.24	-	84.87	-	81.55	-	83.18	-
Res2net101	88.68	+1.44	85.15	+0.28	80.77	-0.78	82.90	-0.28
Res2net101+CSRA (MCANet)	92.35	+5.11	86.40	+1.53	88.20	+6.65	87.29	+4.11

4. 4. 3. Class Activation Mapping for Model Interpretability

In this section, to improve the interpretability of our model’s prediction, we use class activation mapping (CAM) (Zhou et al. 2016) to visualize the spatial regions most influential to the predicted class in the test images, as illustrated in Fig.7. CAM generates a spatial heatmap by using the weights from the final classification layer to linearly combine feature maps from the last convolutional layer, highlighting areas most relevant areas to the predicted class. This method is particularly effective in providing interpretability to deep learning models by revealing the spatial locations that are most influential in the decision-making process. By comparing these visualized heatmaps with the corresponding original images, we validate that the highlighted areas accurately match the relevant regions within the actual scenes. It is noteworthy that our proposed network demonstrates the capability to precisely identify and classify both large-scale features, such as the Building Total Destruction category, and finer details, like Vehicle, which indicates a robust ability to capture multi-scale damage patterns.

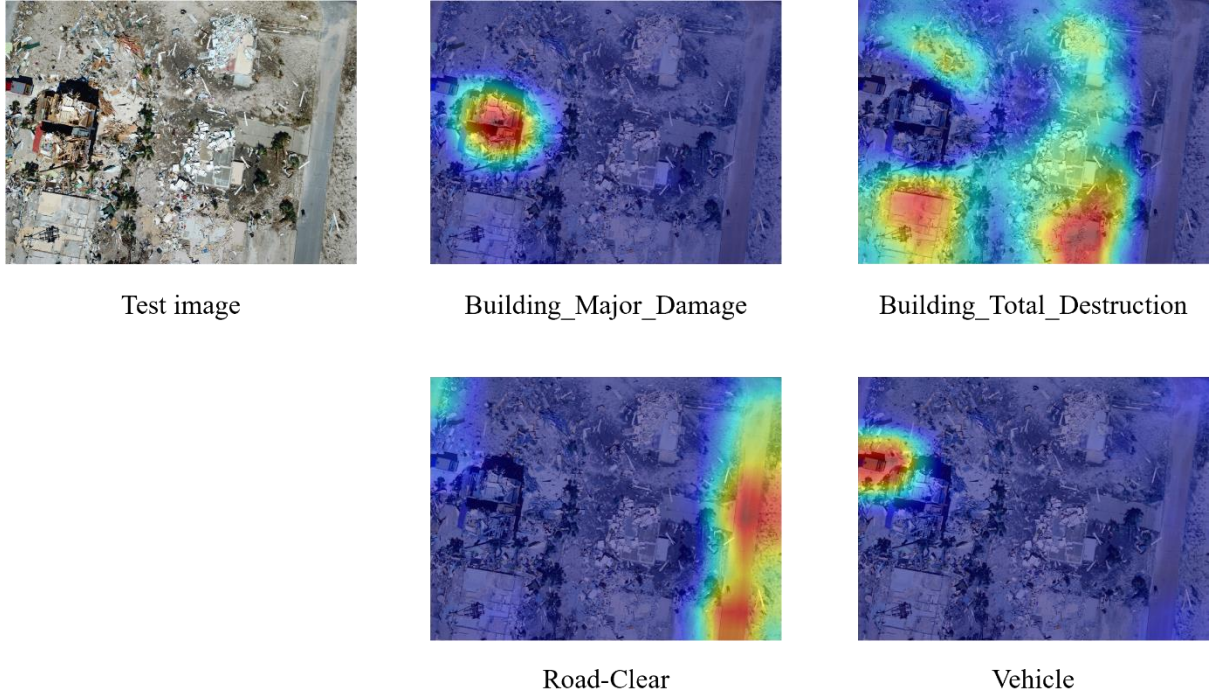


Fig. 7. Visualization results of class activation maps learned by MCANet. Test image (left), attention heat maps and predicted labels (right).

5. Discussion

This study addresses a fundamental gap in post-hurricane damage assessment: the need for an efficient and accurate method for multi-label classification of co-occurring and spatially complex disaster damage patterns in UAV imagery. Existing approaches often rely on single-label classifiers or pixel-level segmentation models, which either oversimplify real-world disaster scenes or incur prohibitive annotation costs. Furthermore, existing CNN-based architectures are limited in their ability to model multi-scale spatial features (Kopiika et al. 2025) and differentiate visually similar classes (Liu et al. 2025a), both of which are crucial in post-disaster contexts.

In response, we introduced MCANet, a multi-label classification architecture that integrates a Res2Net-based hierarchical backbone for multi-scale representation learning with a CSRA module to focus on spatially relevant regions for each damage type. Additionally, we extended the CSRA module with a multi-head mechanism, where each attention head is configured with a distinct temperature parameter. This allows the model to capture

both localized damage patterns and broad contextual features in parallel, enhancing robustness in visually ambiguous or overlapping damage scenarios. Experimental results on the RescueNet dataset validate the effectiveness of our approach. MCANet consistently outperforms a range of strong baselines—including ResNet (He et al. 2016), Res2Net (Gao et al. 2021), VGG (Simonyan and Zisserman 2015), MobileNet (Howard et al. 2017), EfficientNet (Tan and Le 2020), and ViT —achieving a mAP of 91.75% and the highest overall scores across OP, OR, and OF1. The ablation studies validate the complementary effects of the Res2Net backbone and the CSRA module. Notably, the multi-head attention strategy further enhances performance, with mAP improving to 92.35% and AP for the challenging Road Blocked class rising from 71.56% (one head) to 78.13% (eight heads), suggesting that the diverse spatial focus provided by multiple attention heads is especially effective for fragmented and spatially dispersed damage patterns that are difficult to localize. Class Activation Mapping visualizations also demonstrate that MCANet effectively attends to relevant damage regions, from large-scale destruction to fine-grained objects, supporting its interpretability in real-world applications.

Beyond technical contributions, MCANet provides practical value for real-time emergency response and long-term disaster recovery. After a hurricane, fleets of UAVs can rapidly collect aerial imagery over affected areas. MCANet can process these images and produce multi-label outputs based on UAV-captured geospatial context. By aligning damage labels with UAV geolocation data, the system can generate multi-layered risk maps—including estimates of building damage severity, road accessibility, tree obstructions, and flood extent—which allow responders to quickly assess disaster impacts. Furthermore, the structured outputs produced by MCANet can serve as critical input to downstream optimization and decision-support systems. When integrated into digital twin platforms (Mohammadi and Taylor 2017, 2021), these outputs enable dynamic situational awareness and disaster response strategies such as UAV flight path optimization (Hu et al. 2023), response time prediction of emergency medical services (Pan et al. 2024), search-and-rescue priority assignment, and utility restoration

scheduling. For example, by distinguishing between accessible and obstructed road segments while simultaneously evaluating nearby structural damage, MCANet facilitates informed routing of emergency vehicles and prioritization of aid delivery to severely affected zones. This integration helps bridge the gap between damage assessment and actionable response, enabling emergency managers to move from passive damage reporting to data-driven, adaptive deployment strategies.

This study also presents several limitations. First, class imbalance in the RescueNet dataset adversely affects the model’s ability to detect low-frequency categories such as “road blocked” and “building minor damage”, leading to lower recall for these classes. Second, the model relies exclusively on clear UAV imagery, which limits its robustness in visually challenging conditions such as poor lighting and low resolution. To address these limitations and further enhance performance, several directions can be explored. First, class imbalance could be mitigated through targeted data augmentation strategies, such as generating synthetic samples for underrepresented categories (Lu et al. 2025). Second, MCANet can be extended into a multimodal learning framework by integrating complementary data sources, including infrared imagery, social media content, and environmental sensor data, to improve resilience under adverse sensing conditions.

In addition, future research may explore incorporating urban and environmental features (Thomas et al. 2025) through disaster-specific knowledge graphs, enabling the model to reason over contextual relationships between damage types, infrastructure elements, and environmental factors. Such integration could also support zero-shot or few-shot classification of novel damage categories not observed during training, thereby improving the model’s adaptability to new disaster scenarios. Furthermore, the emergence of multimodal large language models offers promising opportunities to combine textual and visual information for enriched semantic understanding, which could enhance both classification accuracy and interpretability in real-world decision-making systems (Ho et al. 2025).

6. Conclusion

This study presents MCANet, a deep learning framework for multi-label post-hurricane damage classification using UAV imagery. By integrating a multi-scale feature extractor Res2Net with class-specific attention mechanism, MCANet effectively distinguishes co-occurring damage types of varying sizes and visual similarity. Experiments on the RescueNet dataset demonstrate that MCANet outperforms a range of baselines including ResNet, Res2Net, VGG, MobileNet, EfficientNet, and ViT, achieving a mAP of 91.75%, and further improves to 92.35% with multi-head attention design. The challenging Road Blocked class has an AP increase of more than 6% compared to the single-head configuration, indicating the benefit of diverse spatial focus patterns. Class activation mapping visualizations confirm the model's ability to accurately localize relevant damage areas from large-scale destruction to fine-grained objects, enhancing model interpretability. MCANet's structured outputs offer practical value for downstream applications such as risk mapping, emergency routing, and disaster decision-making dynamics. Future research may explore extending MCANet with disaster-specific knowledge graphs and multimodal large language models to enhance adaptability to unseen disaster types and deepen semantic reasoning in real-world response scenarios.

Data Availability Statement

The code is publicly available at <https://github.com/ZhangdingLiu/MCANet>.

References

Aela, P., H.-L. Chi, A. Fares, T. Zayed, and M. Kim. 2024. "UAV-based studies in railway infrastructure monitoring." *Automation in Construction*, 167: 105714. <https://doi.org/10.1016/j.autcon.2024.105714>.

- Al Shafian, S., and D. Hu. 2024. "Integrating Machine Learning and Remote Sensing in Disaster Management: A Decadal Review of Post-Disaster Building Damage Assessment." *Buildings*, 14 (8): 2344. Multidisciplinary Digital Publishing Institute. <https://doi.org/10.3390/buildings14082344>.
- Balaguru, K., W. Xu, C.-C. Chang, L. R. Leung, D. R. Judi, S. M. Hagos, M. F. Wehner, J. P. Kossin, and M. Ting. 2023. "Increased U.S. coastal hurricane risk under climate change." *Science Advances*, 9 (14): eadf0259. American Association for the Advancement of Science. <https://doi.org/10.1126/sciadv.adf0259>.
- Berezina, P., and D. Liu. 2022. "Hurricane damage assessment using coupled convolutional neural networks: a case study of hurricane Michael." *Geomatics, Natural Hazards and Risk*, 13 (1): 414–431. Taylor & Francis. <https://doi.org/10.1080/19475705.2022.2030414>.
- Cao, Q. D., and Y. Choe. 2020. "Building damage annotation on post-hurricane satellite imagery based on convolutional neural networks." *Nat Hazards*, 103 (3): 3357–3376. <https://doi.org/10.1007/s11069-020-04133-2>.
- Chen, Z.-M., X.-S. Wei, P. Wang, and Y. Guo. 2019. "Multi-Label Image Recognition with Graph Convolutional Networks." arXiv, arXiv:1904.03582. <http://arxiv.org/abs/1904.03582>.
- Cheng, C.-S., A. H. Behzadan, and A. Noshadravan. 2021. "Deep learning for post-hurricane aerial damage assessment of buildings." *Computer-Aided Civil and Infrastructure Engineering*, 36 (6): 695–710. <https://doi.org/10.1111/mice.12658>.
- Chou, J.-S., S.-C. Hsu, C.-W. Lin, C.-J. Lee, and J.-L. Wei. 2017. "Structural analysis of the relationships between implementing tasks and ex-post effectiveness for disaster mitigation practice in Taipei City." *Sustainable Cities and Society*, 34: 1–11. <https://doi.org/10.1016/j.scs.2017.06.002>.
- Deng, J., Dong, W., Socher, R., Li, L.-J., Li, K., and Fei-Fei, L. 2009. "ImageNet: A large-scale hierarchical image database." Proc., 2009 IEEE Conference on Computer Vision and Pattern Recognition, IEEE, Miami, FL, 248–255.
- Dosovitskiy, A., L. Beyer, A. Kolesnikov, D. Weissenborn, X. Zhai, T. Unterthiner, M. Dehghani, M. Minderer, G. Heigold, S. Gelly, J. Uszkoreit, and N. Houlsby. 2021. "An Image is Worth 16x16 Words: Transformers for Image Recognition at Scale." arXiv, arXiv:2010.11929. <http://arxiv.org/abs/2010.11929>.
- Einizina, S., K. Khoshelham, S. Winter, P. Christopher, Y. Fang, E. Windholz, M. Radanovic, and S. Hu. 2023. "Enabling technologies for remote and virtual inspection of building work." *Automation in Construction*, 156: 105096. <https://doi.org/10.1016/j.autcon.2023.105096>.
- Ejaz, N., and S. Choudhury. 2024. "Computer vision in drone imagery for infrastructure management." *Automation in Construction*, 163: 105418. <https://doi.org/10.1016/j.autcon.2024.105418>.
- Emanuel, K. 2005. "Increasing destructiveness of tropical cyclones over the past 30 years." *Nature*, 436 (7051): 686–688. Nature Publishing Group. <https://doi.org/10.1038/nature03906>.
- Gao, B.-B., and H.-Y. Zhou. 2021. "Learning to Discover Multi-Class Attentional Regions for Multi-Label Image Recognition." *IEEE Trans. on Image Process.*, 30: 5920–5932. <https://doi.org/10.1109/TIP.2021.3088605>.
- Gao, S.-H., M.-M. Cheng, K. Zhao, X.-Y. Zhang, M.-H. Yang, and P. Torr. 2021. "Res2Net: A New Multi-scale Backbone Architecture." *IEEE Trans. Pattern Anal. Mach. Intell.*, 43 (2): 652–662. <https://doi.org/10.1109/TPAMI.2019.2938758>.

- Grinsted, A., P. Ditlevsen, and J. H. Christensen. 2019. "Normalized US hurricane damage estimates using area of total destruction, 1900–2018." *Proceedings of the National Academy of Sciences*, 116 (48): 23942–23946. *Proceedings of the National Academy of Sciences*. <https://doi.org/10.1073/pnas.1912277116>.
- He, K., X. Zhang, S. Ren, and J. Sun. 2016. "Deep Residual Learning for Image Recognition." *2016 IEEE Conference on Computer Vision and Pattern Recognition (CVPR)*, 770–778.
- Ho Ro, S., Y. Li, and J. Gong. 2024. "A Machine learning approach for Post-Disaster data curation." *Advanced Engineering Informatics*, 60: 102427. <https://doi.org/10.1016/j.aei.2024.102427>.
- Ho, Y.-H., L. Li, and A. Mostafavi. 2025. "Integrated vision language and foundation model for automated estimation of building lowest floor elevation." *Computer-Aided Civil and Infrastructure Engineering*, 40 (1): 75–90. <https://doi.org/10.1111/mice.13310>.
- Howard, A. G., M. Zhu, B. Chen, D. Kalenichenko, W. Wang, T. Weyand, M. Andreetto, and H. Adam. 2017. "MobileNets: Efficient Convolutional Neural Networks for Mobile Vision Applications." arXiv, arXiv:1704.04861. <http://arxiv.org/abs/1704.04861>.
- Hu, D., S. Li, J. Du, and J. Cai. 2023. "Automating Building Damage Reconnaissance to Optimize Drone Mission Planning for Disaster Response." *Journal of Computing in Civil Engineering*, 37 (3): 04023006. [https://doi.org/10.1061/\(ASCE\)CP.1943-5487.0001061](https://doi.org/10.1061/(ASCE)CP.1943-5487.0001061).
- Hua, Y., L. Mou, and X. X. Zhu. 2020. "Relation Network for Multilabel Aerial Image Classification." *IEEE Transactions on Geoscience and Remote Sensing*, 58 (7): 4558–4572. <https://doi.org/10.1109/TGRS.2019.2963364>.
- Jing, R., S. Heft-Neal, D. R. Chavas, M. Griswold, Z. Wang, A. Clark-Ginsberg, D. Guha-Sapir, E. Bendavid, and Z. Wagner. 2024. "Global population profile of tropical cyclone exposure from 2002 to 2019." *Nature*, 626 (7999): 549–554. Nature Publishing Group. <https://doi.org/10.1038/s41586-023-06963-z>.
- Kaur, N., C.-C. Lee, A. Mostafavi, and A. Mahdavi-Amiri. 2023. "Large-scale building damage assessment using a novel hierarchical transformer architecture on satellite images." *Computer-Aided Civil and Infrastructure Engineering*, 38 (15): 2072–2091. <https://doi.org/10.1111/mice.12981>.
- Kaur, S., S. Gupta, and S. Singh. 2021. "Hurricane Damage Detection using Machine Learning and Deep Learning Techniques: A Review." *IOP Conf. Ser.: Mater. Sci. Eng.*, 1022 (1): 012035. IOP Publishing. <https://doi.org/10.1088/1757-899X/1022/1/012035>.
- Kennedy, A., A. Copp, M. Florence, A. Gradel, K. Gurley, M. Janssen, J. Kaihatu, D. Krafft, and P. Lynett. 2020. "Hurricane Michael in the Area of Mexico Beach, Florida." *Journal of Waterway, Port, Coastal and Ocean Engineering*, 146. [https://doi.org/10.1061/\(ASCE\)WW.1943-5460.0000590](https://doi.org/10.1061/(ASCE)WW.1943-5460.0000590).
- Klotzbach, P. J., S. G. Bowen, R. Pielke, and M. Bell. 2018. "Continental U.S. Hurricane Landfall Frequency and Associated Damage: Observations and Future Risks." <https://doi.org/10.1175/BAMS-D-17-0184.1>.
- Kopiika, N., A. Karavias, P. Krassakis, Z. Ye, J. Ninic, N. Shakhovska, S. Argyroudis, and S.-A. Mitoulis. 2025. "Rapid post-disaster infrastructure damage characterisation using remote sensing and deep learning technologies: A tiered approach." *Automation in Construction*, 170: 105955. <https://doi.org/10.1016/j.autcon.2024.105955>.
- Li, Y., S. Ye, and I. Bartoli. 2018. "Semisupervised classification of hurricane damage from postevent aerial imagery using deep learning." *JARS*, 12 (4): 045008. SPIE. <https://doi.org/10.1117/1.JRS.12.045008>.
- Liu, B., C. Zhan, C. Guo, X. Liu, and S. Ruan. 2025a. "Efficient remote sensing image classification using the novel STConvNeXt convolutional network." *Sci Rep*, 15 (1): 8406. Nature Publishing Group. <https://doi.org/10.1038/s41598-025-92629-x>.

- Liu, C., S. M. E. Sepasgozar, Q. Zhang, and L. Ge. 2022. "A novel attention-based deep learning method for post-disaster building damage classification." *Expert Systems with Applications*, 202: 770–778. <https://doi.org/10.1016/j.eswa.2022.117268>.
- Liu, Z., N. Mohammadi, and J. E. Taylor. 2025b. "Multi-Label Classification Framework for Hurricane Damage Assessment." arXiv, arXiv:2507.02265. <http://arxiv.org/abs/2507.02265>
- Lu, Y., B. Liu, W. Wei, B. Xiao, Z. Liu, and W. Li. 2025. "Generating synthetic images for construction machinery data augmentation utilizing context-aware object placement." *Developments in the Built Environment*, 21: 100610. <https://doi.org/10.1016/j.dibe.2025.100610>.
- McCarthy, M. J., B. Jessen, M. J. Barry, M. Figueroa, J. McIntosh, T. Murray, J. Schmid, and F. E. Muller-Karger. 2020. "Mapping hurricane damage: A comparative analysis of satellite monitoring methods." *International Journal of Applied Earth Observation and Geoinformation*, 91: 102134. <https://doi.org/10.1016/j.jag.2020.102134>.
- Mohammadi, N., and J. E. Taylor. 2017. "Smart city digital twins." *2017 IEEE Symposium Series on Computational Intelligence (SSCI)*, 1–5.
- Mohammadi, N., and J. E. Taylor. 2021. "Thinking fast and slow in disaster decision-making with Smart City Digital Twins." *Nat Comput Sci*, 1 (12): 771–773. Nature Publishing Group. <https://doi.org/10.1038/s43588-021-00174-0>.
- Pan, X., N. Mohammadi, and J. E. Taylor. 2024. "Predicting the Response Time of Emergency Medical Services during Urban Flooding: From Rule-Based to Data-Driven Approach." *Computing in Civil Engineering 2023*, 272–279. Corvallis, Oregon: American Society of Civil Engineers.
- Park, J. A., X. Liu, C. M. Yeum, S. J. Dyke, M. Midwinter, J. Choi, Z. Chu, T. Hacker, and B. Benes. 2022. "Multioutput Image Classification to Support Postearthquake Reconnaissance." *Journal of Performance of Constructed Facilities*, 36 (6): 04022063. American Society of Civil Engineers. [https://doi.org/10.1061/\(ASCE\)CF.1943-5509.0001755](https://doi.org/10.1061/(ASCE)CF.1943-5509.0001755).
- Pi, Y., N. D. Nath, and A. H. Behzadan. 2021. "Detection and Semantic Segmentation of Disaster Damage in UAV Footage." *Journal of Computing in Civil Engineering*, 35 (2): 04020063. American Society of Civil Engineers. [https://doi.org/10.1061/\(ASCE\)CP.1943-5487.0000947](https://doi.org/10.1061/(ASCE)CP.1943-5487.0000947).
- Pitakaso, R., T. Srichok, S. Khonjun, P. Golinska-Dawson, K. Sethanan, N. Nanthasamroeng, S. Gonwirat, P. Luesak, and C. Boonmee. 2024. "Optimization-driven artificial intelligence-enhanced municipal waste classification system for disaster waste management." *Engineering Applications of Artificial Intelligence*, 133: 108614. <https://doi.org/10.1016/j.engappai.2024.108614>.
- Qi, X., P. Zhu, Y. Wang, L. Zhang, J. Peng, M. Wu, J. Chen, X. Zhao, N. Zang, and P. T. Mathiopoulos. 2020. "MLRSNet: A multi-label high spatial resolution remote sensing dataset for semantic scene understanding." *ISPRS Journal of Photogrammetry and Remote Sensing*, 169: 337–350. <https://doi.org/10.1016/j.isprsjprs.2020.09.020>.
- Rahnemoonfar, M., T. Chowdhury, and R. Murphy. 2023. "RescueNet: A High Resolution UAV Semantic Segmentation Dataset for Natural Disaster Damage Assessment." *Sci Data*, 10 (1): 913. <https://doi.org/10.1038/s41597-023-02799-4>.
- Ro, S. H., and J. Gong. 2024. "Scalable approach to create annotated disaster image database supporting AI-driven damage assessment." *Nat Hazards*, 120 (13): 11693–11712. <https://doi.org/10.1007/s11069-024-06641-x>.
- Salley, C., N. Mohammadi, J. Xie, I. Tien, and J. E. Taylor. 2024. "Assessing Community Needs in Disasters: Transfer Learning for Fusing Limited Georeferenced Data from Crowdsourced Applications on the

- Community Level.” *Journal of Management in Engineering*, 40 (6): 04024055. American Society of Civil Engineers. <https://doi.org/10.1061/JMENEA.MEENG-6208>.
- Shao, Z., K. Yang, and W. Zhou. 2018. “Performance Evaluation of Single-Label and Multi-Label Remote Sensing Image Retrieval Using a Dense Labeling Dataset.” *Remote Sensing*, 10 (6): 964. Multidisciplinary Digital Publishing Institute. <https://doi.org/10.3390/rs10060964>.
- Shao, Z., W. Zhou, X. Deng, M. Zhang, and Q. Cheng. 2020. “Multilabel Remote Sensing Image Retrieval Based on Fully Convolutional Network.” *IEEE Journal of Selected Topics in Applied Earth Observations and Remote Sensing*, 13: 318–328. <https://doi.org/10.1109/JSTARS.2019.2961634>.
- Simonyan, K., and A. Zisserman. 2015. “Very Deep Convolutional Networks for Large-Scale Image Recognition.” Proc., Int. Conf. on Learning Representations (ICLR). <https://arxiv.org/abs/1409.1556>.
- Sirhan, M., S. Bekhor, and A. Sidess. 2024. “Multilabel CNN Model for Asphalt Distress Classification.” *Journal of Computing in Civil Engineering*, 38 (1): 04023040. American Society of Civil Engineers. <https://doi.org/10.1061/JCCEE5.CPENG-5500>.
- Spencer, B. F., V. Hoskere, and Y. Narazaki. 2019. “Advances in Computer Vision-Based Civil Infrastructure Inspection and Monitoring.” *Engineering*, 5 (2): 199–222. <https://doi.org/10.1016/j.eng.2018.11.030>.
- Stoimchev, M., D. Koccev, and S. Džeroski. 2023. “Deep Network Architectures as Feature Extractors for Multi-Label Classification of Remote Sensing Images.” *Remote Sensing*, 15 (2): 538. Multidisciplinary Digital Publishing Institute. <https://doi.org/10.3390/rs15020538>.
- Sumbul, G., M. Charfuelan, B. Demir, and V. Markl. 2019. “BigEarthNet: A Large-Scale Benchmark Archive For Remote Sensing Image Understanding.” *IGARSS 2019 - 2019 IEEE International Geoscience and Remote Sensing Symposium*, 5901–5904.
- Sumbul, G., and B. Demır. 2020. “A Deep Multi-Attention Driven Approach for Multi-Label Remote Sensing Image Classification.” *IEEE Access*, 8: 95934–95946. <https://doi.org/10.1109/ACCESS.2020.2995805>.
- Sun, Z., and Q. Huang. 2023. “Actionable Science for Hurricane.” *Actionable Science of Global Environment Change: From Big Data to Practical Research*, Z. Sun, ed., 111–147. Cham: Springer International Publishing.
- Tan, M., and Q. V. Le. 2020. “EfficientNet: Rethinking Model Scaling for Convolutional Neural Networks.” Proceedings of the 36th International Conference on Machine Learning (ICML), 6105–6114.
- Thomas, M. M., Z. Liu, N. Mohammadi, and J. E. Taylor. 2025. “Parameter Adjustment for Mechanistic Epidemiological Models of COVID-19: Controlling for the Impact of Metro Area Crowding.” Preprint, Version 1, Research Square, <https://doi.org/10.21203/rs.3.rs-7312496/v1>.
- Tong, J., L. Xiang, A. A. Zhang, X. Miao, M. Wang, and P. Ye. 2025. “Fusion of Convolution Neural Network and Visual Transformer for Lithology Identification Using Tunnel Face Images.” *Journal of Computing in Civil Engineering*, 39 (2): 04024056. American Society of Civil Engineers. <https://doi.org/10.1061/JCCEE5.CPENG-5997>.
- Tseng, M.-H. 2023. “GA-based weighted ensemble learning for multi-label aerial image classification using convolutional neural networks and vision transformers.” *Mach. Learn.: Sci. Technol.*, 4 (4): 045045. IOP Publishing. <https://doi.org/10.1088/2632-2153/ad10cf>.
- Wang, J., Y. Yang, J. Mao, Z. Huang, C. Huang, and W. Xu. 2016. “CNN-RNN: A Unified Framework for Multi-label Image Classification.” *2016 IEEE Conference on Computer Vision and Pattern Recognition (CVPR)*, 2285–2294. Las Vegas, NV, USA: IEEE.
- Wang, Q., and J. E. Taylor. 2014. “Quantifying Human Mobility Perturbation and Resilience in Hurricane Sandy.” *PLOS ONE*, 9 (11): e112608. Public Library of Science. <https://doi.org/10.1371/journal.pone.0112608>.

- Wang, Q., and J. E. Taylor. 2016. "Patterns and Limitations of Urban Human Mobility Resilience under the Influence of Multiple Types of Natural Disaster." *PLOS ONE*, 11 (1): e0147299. Public Library of Science. <https://doi.org/10.1371/journal.pone.0147299>.
- Wang, X., L. Duan, and C. Ning. 2021. "Global Context-Based Multilevel Feature Fusion Networks for Multilabel Remote Sensing Image Scene Classification." *IEEE Journal of Selected Topics in Applied Earth Observations and Remote Sensing*, 14: 11179–11196. <https://doi.org/10.1109/JSTARS.2021.3122464>.
- Weinkle, J., C. Landsea, D. Collins, R. Musulin, R. P. Crompton, P. J. Klotzbach, and R. Pielke. 2018. "Normalized hurricane damage in the continental United States 1900–2017." *Nat Sustain*, 1 (12): 808–813. <https://doi.org/10.1038/s41893-018-0165-2>.
- You, H., J. Gu, and W. Jing. 2023. "Multi-Label Remote Sensing Image Land Cover Classification Based on a Multi-Dimensional Attention Mechanism." *Remote Sensing*, 15 (20): 4979. Multidisciplinary Digital Publishing Institute. <https://doi.org/10.3390/rs15204979>.
- Young, R., and S. Hsiang. 2024. "Mortality caused by tropical cyclones in the United States." *Nature*, 635 (8037): 121–128. Nature Publishing Group. <https://doi.org/10.1038/s41586-024-07945-5>.
- Zhou, B., A. Khosla, A. Lapedriza, A. Oliva, and A. Torralba. 2016. "Learning Deep Features for Discriminative Localization." *2016 IEEE Conference on Computer Vision and Pattern Recognition (CVPR)*, 2921–2929.
- Zhou, W., P. Dou, T. Su, H. Hu, and Z. Zheng. 2023. "Feature learning network with transformer for multi-label image classification." *Pattern Recognition*, 136: 109203. <https://doi.org/10.1016/j.patcog.2022.109203>.
- Zhu, K., and J. Wu. 2021. "Residual Attention: A Simple but Effective Method for Multi-Label Recognition." arXiv, arXiv:2108.02456. <http://arxiv.org/abs/2108.02456>.